Nucleic Acids Research Advance Access published May 22, 2013

Nucleic Acids Research, 2013, 1–8
doi:10.1093/nar/gkt425

Structural and torsional properties of the RAD51-dsDNA nucleoprotein filament

Mina Lee[1], Jan Lipfert[1], Humberto Sanchez[2], Claire Wyman[2] and Nynke H. Dekker[1,*]

[1]Department of Bionanoscience, Kavli Institute of Nanoscience, Delft University of Technology, Lorentzweg 1, 2628 CJ Delft, The Netherlands and [2]Department of Genetics, Department of Radiation Oncology, Erasmus University Medical Center, P. O. Box 2040, 3000 CA Rotterdam, The Netherlands

Received March 25, 2013; Revised and Accepted April 25, 2013

ABSTRACT

Human RAD51 is a key protein in the repair of DNA by homologous recombination. Its assembly onto DNA, which induces changes in DNA structure, results in the formation of a nucleoprotein filament that forms the basis of strand exchange. Here, we determine the structural and mechanical properties of RAD51-dsDNA filaments. Our measurements use two recently developed magnetic tweezers assays, freely orbiting magnetic tweezers and magnetic torque tweezers, designed to measure the twist and torque of individual molecules. By directly monitoring changes in DNA twist on RAD51 binding, we determine the unwinding angle per RAD51 monomer to be 45°, in quantitative agreement with that of its bacterial homolog, RecA. Measurements of the torque that is built up when RAD51-dsDNA filaments are twisted show that under conditions that suppress ATP hydrolysis the torsional persistence length of the RAD51-dsDNA filament exceeds that of its RecA counterpart by a factor of three. Examination of the filament's torsional stiffness for different combinations of divalent ions and nucleotide cofactors reveals that the Ca^{2+} ion, apart from suppressing ATPase activity, plays a key role in increasing the torsional stiffness of the filament. These quantitative measurements of RAD51-imposed DNA distortions and accumulated mechanical stress suggest a finely tuned interplay between chemical and mechanical interactions within the RAD51 nucleoprotein filament.

INTRODUCTION

Homologous recombination is an essential process responsible for the accurate repair of DNA double-strand breaks (1). During repair, the defining DNA strand exchange step is catalyzed by proteins (Rad51, RecA or RadA in eukaryotes, bacteria and archaea, respectively) that assemble together with a nucleotide cofactor onto exposed single-stranded DNA (ssDNA) at the damaged site and form a nucleoprotein filament. This helical nucleoprotein filament is the catalytic core of the repair process (2,3); it recognizes a homologous sequence within an intact double-stranded DNA (dsDNA) molecule and promotes ssDNA invasion into the homologous sequence. Recent single-molecule manipulation experiments using filaments of the bacterial homologue RecA assembled on DNA have begun to provide detailed insights on how the filament can slide along a dsDNA target (4), perform 3D homology search (5) and mechanically interact with sites of homology (6). A complete understanding of these processes requires knowledge of both the structure of the filament and of its mechanical properties.

An essential element of promoting homology recognition and strand exchange is the constrained and distorted structure of the bound DNA (7). Electron microscopy (8–10) and radiographic crystallography (11–13) have provided insights into the overall arrangement of nucleoprotein filaments, including the number of protein monomers per helical turn and their positions relative to each other. Structural models derived from radiographic crystallography additionally indicate the arrangement of amino acids that compose the proteins and the location of nucleotide cofactor between the monomers (11–13). The arrangement of DNA within the dsDNA-nucleoprotein filament is best described for RecA where radiographic crystallography has resolved all components: protein, nucleotide and DNA (13). In agreement with previous structural work (7,8) the crystal structure of the full RecA nucleoprotein filament (13) reveals that DNA is lengthened by 1.5-fold and unwound by 45° per RecA monomer compared with regular B-form DNA. To date, estimates of the consequences of RAD51 binding to DNA are not as complete but appear to be similar. Electron microscopy studies (10,14) suggest that the RAD51-dsDNA filament has a rise per base pair of 5.1 Å (compared with 3.4 Å for B-DNA) and 18.6 bp per turn

*To whom correspondence should be addressed. Tel: +31 15 2783219; Fax: +31 15 2781202; Email: n.h.dekker@tudelft.nl

(compared with 10.5 bp per turn for B-DNA), corresponding to an unwinding angle of 45° per RAD51 monomer, in agreement with a modeling study of the RAD51-dsDNA filament (15) based on circular dichroism spectroscopy. However, a single-molecule study that directly monitored RAD51 assembly on dsDNA reported an unwinding angle per monomer of 65 ± 5° (16), considerably different from the values found for the other members of RecA/Rad51 families (8–13).

In addition, the mechanical properties of DNA and the nucleoprotein filaments that are likely to play important roles in promoting homologous recombination have yet to be defined. The nucleoprotein filaments that catalyze strand exchange are observed qualitatively to be stiff and regular, or less stiff and irregular, largely depending on the status of the bound nucleotide cofactor (17,18). Conditions that favor bound ATP and inhibit ATP hydrolysis correlate with stiff and regular filaments (18). In general, polymers such as recombinase nucleoprotein filaments can be characterized by their bending persistence length (L_p) and torsional stiffness. Single-molecule stretching experiments report a value of L_p of ~300 nm for the RAD51-dsDNA filament (19,20), much larger than that of bare dsDNA (~45 nm) (21,22), though smaller than the reported value for the RecA-dsDNA filament (~700 nm) (17,23), respectively. The torsional persistence length (C) quantifies stiffness in terms of twisting. Recently, direct torque measurement of the RecA-dsDNA filaments revealed that C of the filament is ~170 nm (24), which is only modestly higher than the torsional stiffness of dsDNA (C ~90 nm) (24–26). However, for RAD51-DNA filament no direct torque measurements have been reported to date. Here, we use two complementary magnetic tweezers assays, termed freely orbiting magnetic tweezers (26) (FOMT) and magnetic torque tweezers (24) (MTT), that enable direct measurements of single-molecule twist and torque, respectively, to determine the overall structure and mechanical properties of RAD51-dsDNA filaments.

MATERIALS AND METHODS

Buffer conditions

Experiments on dsDNA were carried out in 10 mM Tris–HCl buffer (pH 7.5, Sigma) supplemented with 100 mM NaCl (Sigma) and 5 mM NaN_3 (Sigma). The RAD51 nucleoprotein filaments in the presence of Ca^{2+}-ATP were assembled and measured in 25 mM Tris–HCl buffer (pH 7.5), with 25 mM KCl (Sigma), 1 mM dithiothreitol (DTT) (Sigma), 2 mM $CaCl_2$ (Sigma) and 1 mM ATP (Sigma). Bovine serum albumin (BSA; Sigma) and Triton-X (Sigma) at final concentrations of 0.1–0.5 mg/ml and 0.005–0.02 %, respectively, were added to all the buffers.

The RAD51 nucleoprotein filaments in the presence of the non-hydrolyzable ATP analogue AMPPNP were assembled and measured in 20 mM Tris–HCl buffer (pH 7.5), 50 mM NaCl, 1 mM DTT, 1 mM $CaCl_2$ or $MgCl_2$ (Sigma) and 1 mM AMPPNP (Sigma). The buffer was modified from that used in the Ca^{2+}-ATP experiments to exclude K^+ ions, which have been reported to occupy the same binding sites as Ca^{2+} ions (27). Its presence could therefore potentially complicate comparisons between the different divalent cations. We note that assembly in the presence of the non-hydrolyzable ATP analogue AMPPNP was slow and benefited from mechanical unwinding of dsDNA tether to reach completion. For these reasons, this experimental condition was probed only in the MTT, and not in the FOMT.

To make as direct a comparison of the torsional stiffness of the RAD51 and RecA nucleoprotein filaments (24) as possible, we repeated the experiments that probe the stiffness of the RAD51 nucleoprotein filament in the presence of Mg^{2+}-AMPPNP at a lower pH, in 20 mM 2-(N-morpholino)ethanesulfonic acid buffer (pH 6.2, Sigma). In this way, the only difference in the buffer conditions used for RAD51- and RecA-dsDNA filament assembly, respectively, was the use of AMPPNP for efficient assembly of RAD51 compared with ATPγS used for RecA.

In all experiments, the final concentration of RAD51 used was varied between 100–400 nM, as specified in the main text.

Purification of Human RAD51 protein

Human RAD51 protein was purified as described in (18). The human RAD51 protein was over-expressed in *Escherichia coli*. Cells were lysed in high salt and the clarified lysate was treated with polyethylenimine. After a second clarification, RAD51 was recovered by $(NH_4)_2SO_4$ salting out, and the resuspended pellet was purified by heparin-sepharose chromatography followed by MonoQ chromatography. The protein was dialyzed against 300 mM KCl, 20 mM HEPES-NaOH (pH 7.8), 1 mM EDTA, 2 mM DTT and 10% glycerol, and stored at −80°C.

DNA construct and flow cell assembly

Tether construction and flow-cell assembly followed methods previously described in detail (24,26,28). In brief, we used a 7.9 kb DNA ligated at the ends to ~600 bp DNA polymerase chain reaction fragments that were functionalized with multiple biotin and digoxigenin groups, respectively. Flow cells were made from glass microscope coverslips with parafilm spacers. The bottom surface was coated with nitrocellulose (0.1% w/v in amyl acetate) and flow cells were stored dry. Before measurements, non-magnetic latex beads (Life Sciences) of 1.0 or 3.0 μm diameter were unspecifically attached to the bottom surface by incubation in T200 buffer (10 mM Tris–HCl buffer (pH 7.5) with 200 mM NaCl) for 30 min to function as reference beads. Before addition of the DNA-linked magnetic beads, the bottom surface was functionalized by incubation with 100 μg/ml anti-digoxigenin (Roche) in phosphate buffered saline for 2 h, to provide for DNA attachment, and passivated by incubation for 30 min with 10 mg/ml BSA (Sigma). DNA molecules were attached to streptavidin-coated superparamagnetic beads (Invitrogen) by incubation in T200 buffer. MyOne beads of 1.0 μm diameter and M270 beads of 2.8 μm diameter were used for FOMT

and MTT experiments, respectively. The DNA-tethered superparamagnetic beads were incubated in the flow cell for 1 h in T200 buffer to allow for DNA attachment to the anti-digoxigenin-coated surface. After flushing out unbound DNA-tethered beads, the flow cell was further passivated by incubating for 1–3 h with 10 mg/ml BSA.

For experiments that used marker bead tracking protocol (see below), we used M270 magnetic beads with non-magnetic biotinylated microspheres of 1 μm diameter (Invitrogen) attached as fiducial markers. To attach the fiducial markers, we incubated the flowcell after tethering the DNA-linked beads for 30 min with 300-fold diluted stock of microspheres in T200 buffer and rinsed extensively afterward.

FOMT and MTT experimental configuration

The experimental configurations used in FOMT and MTT were previously described in detail (24,26). Forces were applied using cylindrical permanent magnets with a center aperture. For MTT experiments, the cylindrical magnet was formed by a stack of three magnets (R-06-02-02-G, Supermagnete) for a total thickness of 6 mm, with a diameter of 6 mm and a 2-mm diameter central hole. In the FOMT experiments, a 'flipped stack' configuration of magnets (29,30) was used, in which the bottom magnet was stacked with opposite magnetization direction to achieve higher pulling forces. In the MTT configuration, an additional magnet (S-04-07-N, Supermagnete) was added on one side of the main magnet stack to apply torque. The side magnet had the shape of a solid cylinder, with 4 mm diameter and a height of 7 mm.

A linear stage (PI M-126.PD, Physik Instrumente) was used to change the distance of the magnets from the flow cell. Both the magnets and the flow cell were mounted on manual two-axis (x,y)-micrometer stages, for alignment of the magnet center and the magnetic beads, respectively. Some of the measurements used an additional computer-controlled (x,y)-nanopositioning stage (733.2DD, Physik Instrumente) to move the flow cell over short distances with sub-micrometer precision for fine alignment of the FOMT and to apply feedback to correct for drift. Beads were illuminated using a collimated LED and imaged with a ×100 oil immersion objective (Olympus ACH 100X; numerical aperture = 1.25) connected to a CCD camera (Pulnix TM-6710CL).

The x, y and z position of the beads are determined using conventional tracking algorithms based on cross-correlation analysis. The upward stretching force on the tether was calibrated from the width of the radial fluctuation by applying the equipartition theorem in radial dimension (26,31).

Tracking of the rotation angle of the beads

We use two different protocols to follow the rotation of beads around their tether axis. The first angular tracking strategy involves attaching small non-magnetic beads to the larger magnetic beads to act as fiducial markers and to track rotation angle explicitly by analyzing the camera images (32) (Supplementary Figure S6a). Using fiducial marker beads, however, requires the additional step of attaching the markers, which reduces the number of usable tethers and offline image analysis process on saved images is time-consuming. Alternatively, the rotation angle can be determined simply from the (x, y) position of the bead on the circular annulus that the free rotation of the bead about the tether point traces out (Supplementary Figure S1a) (26,29). The (x, y) position of the bead is transformed to radial and angular coordinates (R, θ) using the position of the center position determined from fitting the circular trace to a circle (Supplementary Figure S6c). However, the determination of rotation angle from the (x, y) position can fail when the contribution from (linear) Brownian motion of the bead in x and y to the angular coordinate is not small compared with the angular motion. While the contribution of linear fluctuations is negligible in the FOMT configuration, it can result in an underestimation of the rotational trap stiffness in the MTT configuration, which depends on tether length, pulling force and the used rotational trap stiffness (29). We used the simple (x, y)-tracking approach in both FOMT and MTT experiments. For the MTT experiments, we used a relatively low rotational trap stiffness of ~300 pN nm/rad, such that the (x, y)-tracking approach is sufficiently accurate and applied the simple correction described in (29).

RESULTS AND DISCUSSION

We used FOMT (26) to monitor the assembly of RAD51 onto dsDNA and to determine the unwinding angle per RAD51 monomer. The basic FOMT assay (26) consists of a DNA molecule tethered between a flow cell surface and a superparamagnetic bead (Figure 1a). A carefully aligned, vertically oriented cylindrical magnet mounted above the flow cell exerts an upward stretching force while not constraining the free rotation of the bead about the tethers axis. The assay is overall similar to the 'free-rotation magnetic tweezers' used by Arata *et al.* (16) with the important difference that the free energy barrier for rotation by a full turn about the tether axis is much less than the thermal energy k_BT in the FOMT (Supplementary Figure S1), while it exceeds k_BT in the 'free-rotation magnetic tweezers' [see Supplementary Figure S1 of (16)].

After preparing a 7.9 kb dsDNA molecule tethered in the FOMT, filament assembly experiments were initiated by flushing in buffer containing RAD51 (at varying concentrations), 1 mM ATP and 2 mM $CaCl_2$ into the flow cell. We use Ca^{2+} as the divalent cation as it inhibits ATP hydrolysis and thereby prevents protein dissociation, resulting in the formation of stable filaments (33,34). Assembly was monitored both by tracking the length increase of the DNA-tether determined from the beads' z-position and by observing unwinding of the DNA determined by tracking the rotation angle about the DNA-tether axis [Figure 1b; note that in the FOMT configuration we determine the rotation angle by simply converting the tracked (x, y)-position on the circular annulus of the bead's free rotation and converting it to angle, see Supplementary Figure S1] (26,29). In assembly

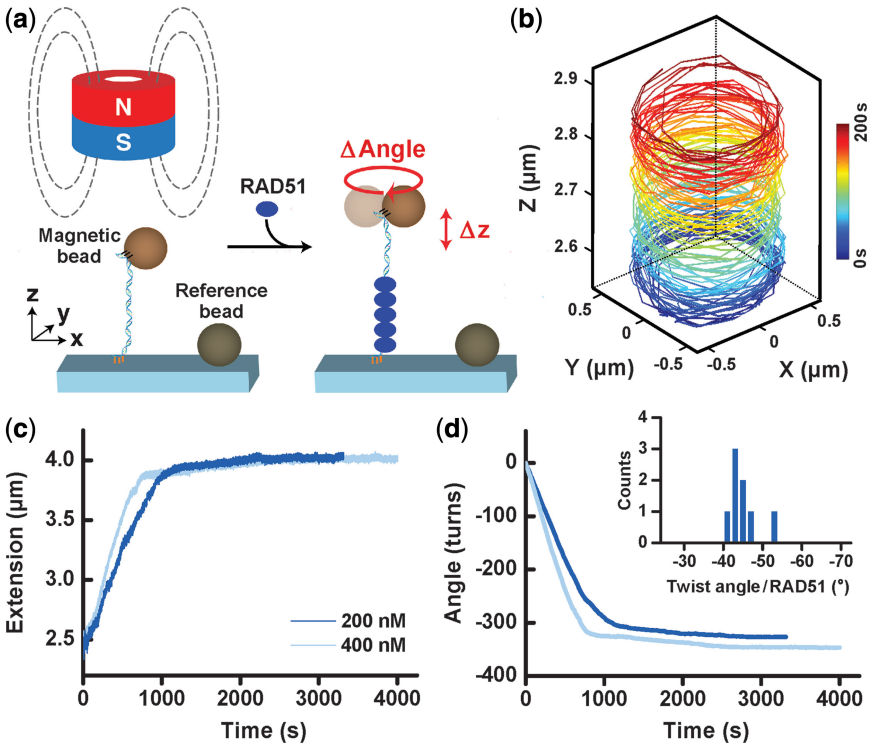

Figure 1. (**a**) Schematic of the FOMT. (**b**) Assembly of RAD51 onto a 7.9 kb dsDNA monitored in the FOMT in the presence of Ca^{2+} and ATP at $F = 3.5$ pN. The (x, y, z) trajectory of the 1.0 μm diameter magnetic bead during the first 200 s of the assembly is shown, with time colour-coded from blue to red. Because RAD51 assembly both unwinds and lengthens the DNA, a spiraling trajectory is observed. (**c**) The extension of the dsDNA [deduced from the z-component of a bead trajectory as shown in (b)] as a function of time for [RAD51] = 200 nM (dark blue) and 400 nM (light blue). (**d**) From the same experiments as shown in (c), the rotation angle about the dsDNA tether axis [deduced from the x, y components of a bead trajectory as shown in (b)] as a function of time. The same colour coding applies as in (c). The inset shows a histogram of the mean twist angle per RAD51 monomer under saturating conditions of RAD51 deduced from measurements on eight distinct DNA molecules.

experiments at relatively high RAD51 concentrations ([RAD51] = 200 or 400 nM), we observed continuous assembly marked by an approximately linear increase in the tether length with time and a concomitant unwinding of the tether (Figure 1c and d). After ~1000 s, assembly went to apparent completion, after which both the tether extension and twist angle remained stable (Figure 1c and d). We determined the contour length L_C and persistence length L_P of the initial bare DNA and the final fully assembled RAD51-dsDNA filament by recording force-extension curves and fitting the data with the worm-like chain model (21) of polymer elasticity (Supplementary Figure S2). We observed a total increase in the contour length from 2.74 ± 0.08 μm to 4.04 ± 0.13 μm and a total unwinding by −313 ± 14 turns (mean and SEM of eight measurements at saturating condition; Supplementary Figure S3). The observed length increase of 1.30 μm corresponds to a 1.47-fold lengthening compared with the initial B-form DNA and is consistent with a 95 ± 11% coverage of the DNA, assuming a length per base pair in the filament of 5.1 Å (10,14). From the total unwinding angle and the coverage, we compute the unwinding angle per RAD51 monomer to be 46° ± 2° (Figure 1d, inset). Alternatively, the unwinding angle per monomer can be computed from the total unwinding angle only, by assuming completely coverage and the stoichiometry of 3 bp per RAD51 monomer (35), resulting in a value of 42° ± 2°, in reasonable agreement with, though likely slightly less accurate than, the estimate taking into account the length information.

When assembly was initiated at lower RAD51 concentration ([RAD51 = 100 nM]), we observed both slower and incomplete assembly that did not reach the same final length and unwinding angle observed at saturating conditions (Supplementary Figure S4). The assembly at higher RAD51 concentration ([RAD51] = 400 nM) in the presence of Mg^{2+} instead of Ca^{2+}, which allows ATP hydrolysis, also showed incomplete coverage and more dynamic assembly behavior (36,37) (Supplementary Figure S5). Nonetheless, using the extension to compute the fractional coverage, we observe an unwinding angle per RAD51 monomer in agreement with the values determined from (near) complete assembly for both cases. Taken together, our FOMT measurements indicate an unwinding angle of ~45° per RAD51 monomer, in agreement with the previous electron microscopy studies of RAD51-DNA filaments (10,14), but in disagreement with the unwinding angle of ~65° per RAD51 monomer measured by Arata *et. al.* (16) The discrepancy may result from the existence of energy barriers to rotational motion that exceeds k_BT in their experimental configuration.

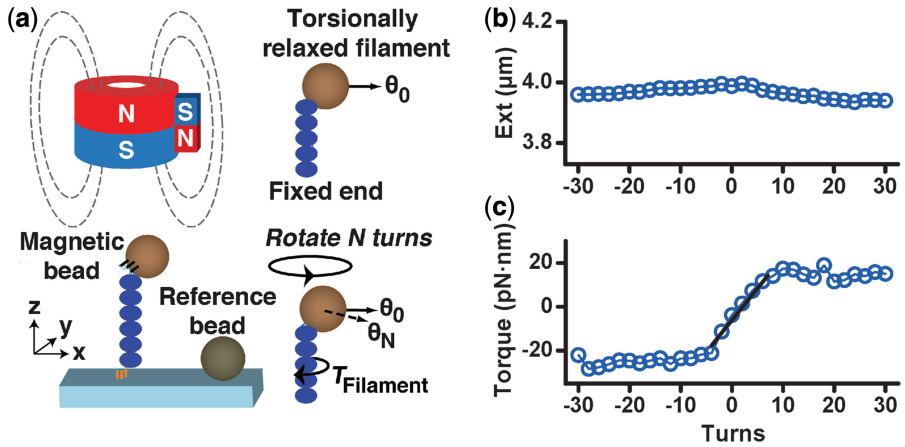

Figure 2. (**a**) Schematic of the MTT. Schematic showing that after overwinding (or underwinding) the RAD51-dsDNA tether by N turns, the tether exerts a restoring torque on the bead that leads to a shift in the equilibrium angular position from θ_0 to θ_N. (**b**) The extension of the complete RAD51-DNA filament as a function of the applied turns at $F = 3.5$ pN following its assembly under same force in the presence of Ca^{2+} and ATP. Zero turns in (b), (**c**) are fixed by the point at which the extension is maximal. (c) From the same experiment as shown in (b), the torque stored in the RAD51-DNA filament as a function of the applied turns.

To probe the response and stability of the RAD51 filaments to torsional strains, we used MTT (24,38) that enable direct measurements of single molecule torque by tracking the rotation angle about the tether axis while holding the bead in a rotational trap (Figure 2a and 'Materials and Methods' section; note that in the MTT we determine the rotation angle either by using a marker bead attached to the larger magnetic bead, or by simply converting the tracked (x, y) to angle as in the FOMT, see Supplementary Figure S6) (24,29). In contrast to the FOMT, in the MTT the rotation of the bead about the tether axis is constrained by the magnets. However, the stiffness of the rotational trap in the MTT remains weak compared with that of conventional magnetic tweezers, facilitating torque measurement (24,29).

RAD51-dsDNA filaments were preassembled in the same buffer as used in the FOMT measurement. During filament assembly, the magnet was rotated by ~−310 turns (34) to relieve the accumulated torsional strain. Subsequently, the extension of the RAD51 filament (Figure 2b) and the torque stored in the filament (Figure 2c) were simultaneously measured as a function of turns. We note that in both curves 'zero' turns was determined from the location in turns at which the extension of the filament is maximal (Figure 2b). As the maximum of the rotation-extension curve for RAD51-dsDNA filaments is relatively shallow (Figure 2b), the achievable accuracy in the estimation of this rotational offset was at most ±2 turns. This results in an uncertainty in the measurement of the absolute torque values of ±8 pN nm (Supplementary Figure S7); the relative torque, however, can be measured with a precision of ±2 pN nm.

Over- and underwinding RAD51 filaments assembled in the presence of ATP and Ca^{2+}, we initially observe a linear response of the torque with the applied number of turns (Figure 2c; zero turns corresponds to the torsionally relaxed filaments). In the linear response regime, the torque after N turns equals $2\pi N k_B T C/L_C$ and we determine the torsional persistence length C of the filament from linear fits to the torque versus turn response (Figure 2c, solid lines). For RAD51-dsDNA filaments assembled in the presence of ATP and Ca^{2+}, we found $C = 504 \pm 57$ nm (mean and SEM from four measurements) at a stretching force of 3.5 pN (blue data in Figure 3c and Supplementary Figure S7).

On further over- or underwinding, the torque eventually saturates and remains constant. We observe torque saturation on under- and overwinding at −20 ± 13 pN nm and 24 ± 14 pN nm, respectively. The large variability in these measurements was mostly due to the inaccuracy of the rotational offset; the difference between the two plateaus, 43 ± 4 pN nm (which is independent of the turn offset) showed substantially lower variability (Supplementary Figure S7a, b). Torque saturation is not likely due to a buckling transition and the formation of plectonemes, as is the case for overwound bare DNA (22,39), as the tether extension remains approximately constant on over- and underwinding into the torque plateau regime (Figure 2b). Instead, the observation that the differences of plateau torques are close to the values previously observed for structural transition of B-form DNA, namely melting on underwinding and the B-to-P-form transition on overwinding (39), respectively, suggests that when twisted beyond the elastic regime, the filament is locally disrupted by torsional stresses and that the DNA within the nucleoprotein filament locally melts or forms P-form DNA. However, other mechanisms for the relaxation of torsional strain, e.g. conformational changes of the proteins or of the protein–DNA interfaces, may also exist. For example, the values of the plateaus at positive turns in the data set with Mg^{2+}-AMPPNP at pH 6.2 (17 ± 7 pN nm) were considerably lower than those observed at pH 7.5 (32 ± 7 pN nm, Supplementary Figure S9), suggesting that the torsional strain induces structural transitions that involve not only local stretches

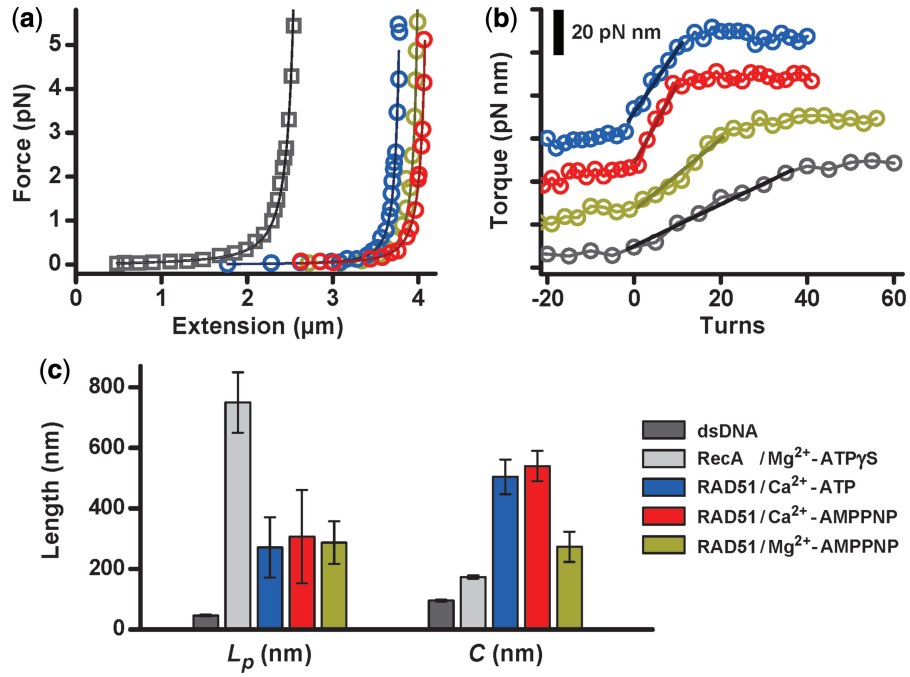

Figure 3. (Same colour code used in all panels.) (**a**) Force-extension curves of bare DNA (dark grey) and RAD51-DNA filament assembled at $F = 3.5$ pN in the presence of Ca^{2+}-ATP (blue), Ca^{2+}-AMPPNP (red) and Mg^{2+}-AMPPNP (dark yellow). The fits of the worm-like chain model (solid lines) yield contour lengths (L_c) and bending persistence lengths (L_p). (**b**) Torque curves as a function of applied turns for bare DNA and for RAD51-DNA filaments assembled under these three conditions. Fits to the linear regime (solid lines) yield the torsional persistence length C. (**c**) Summary of the mean values for L_p and C deduced for bare DNA, RecA-DNA filaments assembled in the presence of Mg^{2+}-ATPγS (grey) and RAD51-DNA filaments assembled under these three conditions.

of bare DNA. However, for the majority of our data sets, the transitions involving local B-DNA appear to be the most likely attribution.

To investigate how different nucleotide cofactors and divalent ions impact the mechanical properties of the RAD51-dsDNA filament, we systematically assembled filaments in buffers with different combinations of nucleotide cofactors and divalent ions. RAD51-dsDNA filaments will assemble in the presence of either ATP or non-hydrolyzable ATP analogues (18,19). However, assembly in conditions of active ATP hydrolysis (e.g. with Mg^{2+}-ATP) resulted in less stable filaments with a variable fraction of protein coverage (Supplementary Figure S5). In practice, the dynamic nature of filaments under conditions where ATP hydrolysis is possible makes reliable torque measurements challenging. Therefore, we performed all torque measurements in conditions under which ATP hydrolysis is suppressed and stable filaments are formed, e.g. in the presence of Ca^{2+}-ATP as above, or in the presence of the non-hydrolyzable ATP analogue AMPPNP. The results of force-extension stretching experiments and torque measurements on filaments assembled in the Ca^{2+}-ATP, Ca^{2+}-AMPPNP and Mg^{2+}-AMPPNP conditions are shown in Figure 3 and Supplementary Figures S7–9. For comparison, we also show the results of experiments on B-DNA (Figure 3, black data) and on RecA-dsDNA filament assembled in Mg^{2+}-ATPγS (24) (Figure 3, grey data). From force-extension measurements (Figure 3a), we determined the contour length (L_c) and bending persistence length (L_p) and found similar values for all three cofactor conditions. The observed bending persistence length values (Figure 3a and left panel of Figure 3c) of ~300 nm are consistent with previous measurements (19,20) and indicate that the bending stiffness of RAD51-dsDNA filaments is ~6-fold larger than that of bare DNA (21,22), yet 2-fold lower than that observed for RecA filaments (17,23). From torque-rotation measurements (Figure 3b and right panel of Figure 3c), we determined the torsional persistence lengths (C) of the RAD51 filaments, which were found to be significantly higher than that of bare DNA (24) under all conditions (Figure 3c). Notably, when Ca^{2+} was substituted for Mg^{2+} in RAD51 filament assembly, the torsional stiffness of the resulting nucleoprotein filament doubled (compare RAD51 assembly in Ca^{2+}-AMPPNP versus Mg^{2+}-AMPPNP in Figure 3b; similarly high values of the torsional stiffness were obtained for assembly in Ca^{2+}-ATP). This suggests that the identity of the divalent ions plays an important role in determining the torsional stiffness of the RAD51-dsDNA filament. In all cases, the torsional stiffness of the RAD51 filament exceeded that of the RecA filament (Figure 3c), with the most direct comparison being possible when the two filaments were assembled under similar conditions (Mg^{2+}-AMPPNP for RAD51, Mg^{2+}-ATPγS for RecA). A final control of RAD51 filament assembly in the presence of Mg^{2+}-AMPPNP but now under acidic buffer conditions (pH 6.2) similar to the optimal assembly conditions for RecA filaments (24), confirmed this trend (Supplementary Figure S9).

To understand how a change in the divalent cation could account for a change in torsional stiffness of the RAD51 filament, we refer to insights into the positioning of divalent ions from structural and modeling studies. To start, the crystal structures of the Rad51 filaments indicate that the ATPase site is located at the interface between monomers of the filament (11,12). As a divalent ion is complexed with a nucleotide cofactor at the ATPase site, it is plausible that the coordination of divalent ions with different sizes might affect the conformation of this site. The conformation of the ATPase site at the interface could subsequently impact the filament structure, protein association with DNA and the resulting DNA mechanical response. Studies of archaeal Rad51 (40) and the meiosis-specific analogue DMC1 (41) suggest an additional binding site for divalent ions that is in proximity to, yet distinct from the ATPase site. Both modeling studies of RAD51 (42) and crystal structures of archaeal Rad51 (40) indicate that Ca^{2+} binding to this site could, by inducing a more ordered conformation of the L2 loop, which is the putative DNA-binding domain, stabilize the nucleoprotein filament. The observation that Mg^{2+} does not induce such changes was attributed to the smaller size and different coordination chemistry compared with Ca^{2+}. Thus, it is conceivable that Ca^{2+}-induced changes in loop L2 would contribute to a stronger interaction with DNA and result in an increased torsional stiffness of the RAD51-dsDNA filament.

Our direct comparison between the mechanical properties of RAD51-dsDNA and RecA-dsDNA filaments touches on two important points. First, when RAD51-dsDNA filaments are assembled at high RAD51 concentration as in our experiments, they do not adopt a fully continuous form but rather consist of protein filaments that are interrupted by short segments of bare DNA, a consequence of the relatively high nucleation rate with respect to the growth rate (20,36,37). Our reported values for the bending and torsional persistence lengths should, therefore, be viewed as effective quantities. Possibly, their values may be slightly lower than those for fully continuous filaments. In this light, it is all the more significant that the torsional stiffness of the RAD51-dsDNA filaments exceeds those of their RecA-dsDNA counterparts, for which such discontinuities occur less frequently (20). Second, the comparison between these two nucleoprotein filaments also illustrates an important conceptual point, namely that a filament's bending stiffness and its torsional stiffness are *a priori* independent quantities. While the torsional stiffness of RAD51-dsDNA filaments is observed to be up to ~3 times larger than that of RecA-dsDNA filaments, the bending persistence length of the RAD51 filaments was substantially lower compared with that of RecA filaments (Figure 3c). The contrasting trends in bending and torsional persistence lengths might be caused by differences in the DNA-binding interaction for the two proteins. For example, in the case of RAD51, Tyr-232 within the L1 loop is proposed to intercalate into the double helix (15), while such interactions are not observed in the structure of RecA-DNA filament (13).

CONCLUSION

We have shown how the simultaneous tracking of the extension and twist of nucleic acids has allowed us to investigate the structure of dsDNA within the RAD51-dsDNA filament. Furthermore, we report direct measurements of the torsional properties of RAD51-dsDNA filaments that reveal a significant effect of the divalent ion cofactors. As these divalent cations are involved in chemistry, our results demonstrate a delicate interplay between chemical and mechanical interactions within the RAD51-dsDNA filament. The methods introduced here are generally applicable and we expect that they can be extended to the study of a wide variety of DNA–protein interactions that are sensitive to DNA torque and twist (43).

SUPPLEMENTARY DATA

Supplementary Data are available at NAR Online: Supplementary Figures 1–9.

ACKNOWLEDGEMENTS

We thank Matthew Wiggin for preliminary experiments and Xander Janssen for useful discussions.

FUNDING

A Vici grant from the Netherlands Organisation for Scientific Research (NWO) and a grant from NanoNextNL, a micro and nano-technology consortium of the Dutch Government and 130 partners to C.W.: a Marie Curie Reintegration grant [FP7-276898 to H.S.]; a Veni grant from NWO to J.L.; a EURYI grant from the European Science Foundation to N.H.D. Funding for open access charge: European Science Foundation.

Conflict of interest statement. None declared.

REFERENCES

1. San Filippo,J., Sung,P. and Klein,H. (2008) Mechanism of eukaryotic homologous recombination. *Annu. Rev. Biochem.*, **77**, 229–257.
2. Baumann,P. and West,S.C. (1998) Role of the human RAD51 protein in homologous recombination and double-stranded-break repair. *Trends Biochem. Sci.*, **23**, 247–251.
3. Holthausen,J.T., Wyman,C. and Kanaar,R. (2010) Regulation of DNA strand exchange in homologous recombination. *DNA Repair (Amst.)*, **9**, 1264–1272.
4. Ragunathan,K., Liu,C. and Ha,T. (2012) RecA filament sliding on DNA facilitates homology search. *eLife*, **1**, e00067.
5. Forget,A.L. and Kowalczykowski,S.C. (2012) Single-molecule imaging of DNA pairing by RecA reveals a three-dimensional homology search. *Nature*, **482**, 423–427.
6. De Vlaminck,I., van Loenhout,M.T., Zweifel,L., den Blanken,J., Hooning,K., Hage,S., Kerssemakers,J. and Dekker,C. (2012) Mechanism of homology recognition in DNA recombination from dual-molecule experiments. *Mol. Cell*, **46**, 616–624.

7. Yu,X., VanLoock,M.S., Yang,S., Reese,J.T. and Egelman,E.H. (2004) What is the structure of the RecA-DNA filament? *Curr. Protein Pept. Sci.*, **5**, 73–79.
8. Story,R.M., Weber,I.T. and Steitz,T.A. (1992) The structure of the *E. coli* recA protein monomer and polymer. *Nature*, **355**, 318–325.
9. Ogawa,T., Yu,X., Shinohara,A. and Egelman,E.H. (1993) Similarity of the yeast RAD51 filament to the bacterial RecA filament. *Science*, **259**, 1896–1899.
10. Benson,F.E., Stasiak,A. and West,S.C. (1994) Purification and characterization of the human Rad51 protein, an analogue of *E. coli* RecA. *EMBO J.*, **13**, 5764–5771.
11. Wu,Y., He,Y., Moya,I.A., Qian,X. and Luo,Y. (2004) Crystal structure of archaeal recombinase RADA: a snapshot of its extended conformation. *Mol. Cell*, **15**, 423–435.
12. Conway,A.B., Lynch,T.W., Zhang,Y., Fortin,G.S., Fung,C.W., Symington,L.S. and Rice,P.A. (2004) Crystal structure of a Rad51 filament. *Nat. Struct. Mol. Biol.*, **11**, 791–796.
13. Chen,Z., Yang,H. and Pavletich,N.P. (2008) Mechanism of homologous recombination from the RecA-ssDNA/dsDNA structures. *Nature*, **453**, 489–484.
14. Yu,X., Jacobs,S.A., West,S.C., Ogawa,T. and Egelman,E.H. (2001) Domain structure and dynamics in the helical filaments formed by RecA and Rad51 on DNA. *Proc. Natl Acad. Sci. USA*, **98**, 8419–8424.
15. Reymer,A., Frykholm,K., Morimatsu,K., Takahashi,M. and Nordén,B. (2009) Structure of human Rad51 protein filament from molecular modeling and site-specific linear dichroism spectroscopy. *Proc. Natl Acad. Sci. USA*, **106**, 13248–13253.
16. Arata,H., Dupont,A., Miné-Hattab,J., Disseau,L., Renodon-Cornière,A., Takahashi,M., Viovy,J.L. and Cappello,G. (2009) Direct observation of twisting steps during Rad51 polymerization on DNA. *Proc. Natl Acad. Sci. USA*, **106**, 19239–19244.
17. Hegner,M., Smith,S.B. and Bustamante,C. (1999) Polymerization and mechanical properties of single RecA-DNA filaments. *Proc. Natl Acad. Sci. USA*, **96**, 10109–10114.
18. Ristic,D., Modesti,M., van der Heijden,T., van Noort,J., Dekker,C., Kanaar,R. and Wyman,C. (2005) Human Rad51 filaments on double- and single-stranded DNA: correlating regular and irregular forms with recombination function. *Nucleic Acids Res.*, **33**, 3292–3302.
19. Miné,J., Disseau,L., Takahashi,M., Cappello,G., Dutreix,M. and Viovy,J.L. (2007) Real-time measurements of the nucleation, growth and dissociation of single Rad51-DNA nucleoprotein filaments. *Nucleic Acids Res.*, **35**, 7171–7187.
20. van der Heijden,T., Seidel,R., Modesti,M., Kanaar,R., Wyman,C. and Dekker,C. (2007) Real-time assembly and disassembly of human RAD51 filaments on individual DNA molecules. *Nucleic Acids Res.*, **35**, 5646–5657.
21. Bouchiat,C., Wang,M.D., Allemand,J., Strick,T., Block,S.M. and Croquette,V. (1999) Estimating the persistence length of a worm-like chain molecule from force-extension measurements. *Biophys. J.*, **76**, 409–413.
22. Forth,S., Deufel,C., Sheinin,M.Y., Daniels,B., Sethna,J.P. and Wang,M.D. (2008) Abrupt buckling transition observed during the plectoneme formation of individual DNA molecules. *Phys. Rev. Lett.*, **100**, 148301.
23. Shivashankar,G.V., Feingold,M., Krichevsky,O. and Libchaber,A. (1999) RecA polymerization on double-stranded DNA by using single-molecule manipulation: the role of ATP hydrolysis. *Proc. Natl Acad. Sci. USA*, **96**, 7916–7921.
24. Lipfert,J., Kerssemakers,J.W., Jager,T. and Dekker,N.H. (2010) Magnetic torque tweezers: measuring torsional stiffness in DNA and RecA-DNA filaments. *Nat. Methods*, **7**, 977–980.
25. Mosconi,F., Allemand,J.F., Bensimon,D. and Croquette,V. (2009) Measurement of the torque on a single stretched and twisted DNA using magnetic tweezers. *Phys. Rev. Lett.*, **102**, 078301.
26. Lipfert,J., Wiggin,M., Kerssemakers,J.W., Pedaci,F. and Dekker,N.H. (2011) Freely orbiting magnetic tweezers to directly monitor changes in the twist of nucleic acids. *Nat. Commun.*, **2**, 439.
27. Wu,Y., Qian,X., He,Y., Moya,I.A. and Luo,Y. (2005) Crystal structure of an ATPase-active form of Rad51 homolog from Methanococcus voltae. Insights into potassium dependence. *J. Biol. Chem.*, **280**, 722–728.
28. Lipfert,J., Koster,D.A., Vilfan,I.D., Hage,S. and Dekker,N.H. (2009) Single-molecule magnetic tweezers studies of type IB topoisomerases. *Methods Mol. Biol.*, **582**, 71–89.
29. Janssen,X.J., Lipfert,J., Jager,T., Daudey,R., Beekman,J. and Dekker,N.H. (2012) Electromagnetic torque tweezers: a versatile approach for measurement of single-molecule twist and torque. *Nano Lett.*, **12**, 3634–3639.
30. Kauert,D.J., Kurth,T., Liedl,T. and Seidel,R. (2011) Direct mechanical measurements reveal the material properties of three-dimensional DNA origami. *Nano Lett.*, **11**, 5558–5563.
31. te Velthuis,A.J., Kerssemakers,J.W., Lipfert,J. and Dekker,N.H. (2010) Quantitative guidelines for force calibration through spectral analysis of magnetic tweezers data. *Biophys J.*, **99**, 1292–1302.
32. Lipfert,J., Kerssemakers,J.J., Rojer,M. and Dekker,N.H. (2011) A method to track rotational motion for use in single-molecule biophysics. *Rev. Sci. Instrum.*, **82**, 103707.
33. Bugreev,D.V. and Mazin,A.V. (2004) Ca^{2+} activates human homologous recombination protein Rad51 by modulating its ATPase activity. *Proc. Natl Acad. Sci. USA*, **101**, 9988–9993.
34. Atwell,S., Disseau,L., Stasiak,A.Z., Stasiak,A., Renodon-Cornière,A., Takahashi,M., Viovy,J.L. and Cappello,G. (2012) Probing Rad51-DNA interactions by changing DNA twist. *Nucleic Acids Res.*, **40**, 11769–11776.
35. Egelman,E.H. (2001) Does a stretched DNA structure dictate the helical geometry of RecA-like filaments? *J. Mol. Biol.*, **309**, 539–542.
36. van Mameren,J., Modesti,M., Kanaar,R., Wyman,C., Peterman,E.J. and Wuite,G.J. (2009) Counting RAD51 proteins disassembling from nucleoprotein filaments under tension. *Nature*, **457**, 745–748.
37. Modesti,M., Ristic,D., van der Heijden,T., Dekker,C., van Mameren,J., Peterman,E.J., Wuite,G.J., Kanaar,R. and Wyman,C. (2007) Fluorescent human RAD51 reveals multiple nucleation sites and filament segments tightly associated along a single DNA molecule. *Structure*, **15**, 599–609.
38. Celedon,A., Nodelman,I.M., Wildt,B., Dewan,R., Searson,P., Wirtz,D., Bowman,G.D. and Sun,S.X. (2009) Magnetic tweezers measurement of single molecule torque. *Nano Lett.*, **9**, 1720–1725.
39. Sheinin,M.Y. and Wang,M.D. (2009) Twist-stretch coupling and phase transition during DNA supercoiling. *Phys. Chem. Chem. Phys.*, **11**, 4800–4803.
40. Qian,X., He,Y., Ma,X., Fodje,M.N., Grochulski,P. and Luo,Y. (2006) Calcium stiffens archaeal Rad51 recombinase from Methanococcus voltae for homologous recombination. *J. Biol. Chem.*, **281**, 39380–39387.
41. Bugreev,D.V., Golub,E.I., Stasiak,A.Z., Stasiak,A. and Mazin,A.V. (2005) Activation of human meiosis-specific recombinase Dmc1 by Ca^{2+}. *J. Biol. Chem.*, **280**, 26886–26895.
42. Fornander,L.H., Frykholm,K., Reymer,A., Renodon-Cornière,A., Takahashi,M. and Nordén,B. (2012) Ca^{2+} improves organization of single-stranded DNA bases in human Rad51 filament, explaining stimulatory effect on gene recombination. *Nucleic Acids Res.*, **40**, 4904–4913.
43. Bryant,Z., Oberstrass,F.C. and Basu,A. (2012) Recent developments in single-molecule DNA mechanics. *Curr. Opin. Struct. Biol.*, **22**, 304–312.